Research article

Journal of RAMAN SPECTROSCOPY

Received: 22 March 2015 Revised: 4 June 2015 Accepted: 4 June 2015 Published online in Wiley Online Library: 8 July 2015

(wileyonlinelibrary.com) DOI 10.1002/jrs.4751

Approximate chemical analysis of volcanic glasses using Raman spectroscopy

Danilo Di Genova,[a]* Daniele Morgavi,[a,b] Kai-Uwe Hess,[a] Daniel R. Neuville,[c] Nikita Borovkov,[a] Diego Perugini[b] and Donald B. Dingwell[a]

The effect of chemical composition on the Raman spectra of a series of natural calcalkaline silicate glasses has been quantified by performing electron microprobe analyses and obtaining Raman spectra on glassy filaments (~450 μm) derived from a magma mingling experiment. The results provide a robust compositionally-dependent database for the Raman spectra of natural silicate glasses along the calcalkaline series. An empirical model based on both the acquired Raman spectra and an ideal mixing equation between calcalkaline basaltic and rhyolitic end-members is constructed enabling the estimation of the chemical composition and degree of polymerization of silicate glasses using Raman spectra. The model is relatively insensitive to acquisition conditions and has been validated using the MPI-DING geochemical standard glasses[1] as well as further samples. The methods and model developed here offer several advantages compared with other analytical and spectroscopic methods such as infrared spectroscopy, X-ray fluorescence spectroscopy, electron and ion microprobe analyses, inasmuch as Raman spectroscopy can be performed with a high spatial resolution (1 μm^2) without the need for any sample preparation as a nondestructive technique. This study represents an advance in efforts to provide the first database of Raman spectra for natural silicate glasses and yields a new approach for the treatment of Raman spectra, which allows us to extract approximate information about the chemical composition of natural silicate glasses using Raman spectroscopy. We anticipate its application in handheld *in situ* terrestrial field studies of silicate glasses under extreme conditions (e.g. extraterrestrial and submarine environments). © 2015 The Authors Journal of Raman Spectroscopy Published by John Wiley & Sons Ltd

Additional supporting information may be found in the online version of this article at the publisher's web site.

Keywords: natural silicate glasses; chemical analysis; volcanology; planetary science; identification

Introduction

Raman spectroscopy provides information about the molecular vibrations of the investigated sample. Since the discovery of the Raman Effect (1928) in scattered light from liquids, Raman spectroscopy has been successfully applied to the analysis of a wide range of materials and systems across the life, earth and planetary, material and chemical sciences, and across our cultural heritage.[2–10]

This spectroscopic technique offers several advantages over other spectroscopic and analytical methods as infrared spectroscopy, X-ray fluorescence, and electron and ion microprobe. Little or no sample preparation is required, and the technique has a nondestructive character. Furthermore, in Raman spectroscopy, the minimum analyzed sample volume is comparable with the activated volume probed by most other spectroscopic and analytic methods.

The acquired Raman spectra can be used to quickly and precisely determine the presence of different compounds (organic and inorganic materials, glasses, minerals, volatiles, liquids, and fluids) with a high resolution, down to 1 μm^2. Thanks to its high spectral and spatial resolution, Raman spectroscopy is widely used for generating detailed chemical maps of heterogeneous samples (if a small pinhole is used).

Additionally, as the excitation source in a Raman apparatus lies in the visible range of light (laser), Raman spectroscopy has been widely used to study buried or included samples in opaque or transparent samples. The laser can penetrate the surface and is scattered into deeper regions, permitting the study of multilayer samples. Detailed chemical and physical characterization of a heterogeneous and multilayer sample is of prime importance as the physical and chemical properties of a heterogeneous sample depend on the spatial distribution of their chemical components, which are easily detected, and located, using Raman spectroscopy.

Recently, Raman apparatus have been used to perform *in situ* analysis for the investigation of archeological glasses and to perform remotely operated analysis at extreme conditions (i.e. submarine and extraterrestrial).[11–16] For example, Pasteris *et al.*[17] presented the first deep ocean Raman *in situ* spectrometer (DORISS) employed for studying the mineralogy of the sea floor and the chemistry of pore water, gas seeps, and sea floor vents. Additionally, the European

* *Correspondence to: Danilo Di Genova, Department of Earth and Environmental Sciences, Ludwig-Maximilians-Universität (LMU), Theresienstrasse 41/III, 80333 München, Germany.*
E-mail: danilo.digenova@min.uni-muenchen.de

The copyright line for this article was changed on 03 September 2015 after original publication.

a *Department of Earth and Environmental Sciences, Ludwig-Maximilians-Universität (LMU), Theresienstrasse 41/III, 80333, München, Germany*

b *Department of Earth Sciences, University of Perugia, Piazza Università, 06100, Perugia, Italy*

c *Géomatériaux, CNRS-IPGP UMR 7154, Paris Sorbonne Cité, 1 rue Jussieu, 75005, Paris, France*

Space Agency has established the ExoMars program (2016–2018) to investigate the Martian environment. The ExoMars rover, which is currently in its design phase, will be equipped with a Raman spectrometer to identify any potential organic compounds, and by the analysis of Martian rocks, to provide information about igneous, metamorphous, and sedimentary processes on the planet. Raman spectroscopy represents a fundamental tool in planetary science, as it can be utilized to (1) identify the presence, and recognize the morphology, of organic and inorganic material; (2) distinguish different compounds within those materials; (3) determine the oxidation state of planetary elements; and (4) to study volatiles and gaseous inclusions within minerals and glasses (see Tarcea *et al.*[5] for detailed applications). Moreover, in comparison with other spectroscopic techniques, Raman spectroscopy appears to be the most suitable technique for sample identification and characterization from orbital remote sensing and surface-remote exploration. This aspect has clearly a great fundamental and practical importance for the identification, and characterization, of heterogeneous samples (i.e. soils and rocks) in remote conditions.

In petrology and volcanology, Raman spectroscopy has typically been used to rapidly investigate and identify mineral phases at very high sensitivity.[18–20] Furthermore, studies have shown that Raman measurements provide information concerning the amorphous structure of synthetic silica glasses demonstrating that with Raman spectroscopy it is possible to discriminate between glass and crystalline materials easily and rapidly.[21–25] This aspect, together with the recent development of portable Raman apparatus, might take on great importance for the *in situ* identification, and investigation, of silicate glasses in volcanic deposits. Additionally, Raman spectroscopy has been applied to the study of fluid and glass inclusions trapped in crystals during magmatic processes.[26–28] Recently, several studies[29–33] have also demonstrated the potential use of Raman spectroscopy for the quantification of water and CO_2 contents in silicate glasses.

In the last few years, the number of scientific publications including review papers relevant to Raman spectroscopy has grown rapidly resulting in part from the development of lasers, charge-coupled devices, and confocal systems.[10,27,34] However, despite the recent advances in Raman spectroscopy and the substantial amount of data produced in the past decades, there is still no unanimous consensus concerning the interpretation of the Raman spectra of natural glasses.[10] Additionally, the application of the quantitative data available from experiments performed on simple systems to natural systems has been quite limited.

In this study, we combine electron microprobe microanalysis with a high spatial resolution (1 μm^2) Raman spectroscopic investigation. The samples consist of the products of a magma mingling/mixing experiment between calcalkaline basaltic and rhyolitic melts. We track the evolution of the Raman spectra as a function of the chemical composition of these natural silicate glasses. We provide, for the first time, a database of Raman spectra of natural glasses combined with an accurate chemical characterization. The evolution of the acquired Raman spectra has been parameterized to provide a Raman model for determining both the degree of polymerization and the approximate chemical composition of silicate glasses for calcalkaline composition. Our approach use a novel spectra characterization that differs from the as yet highly controversial deconvolution procedures previously attempted.[10,34]

Here, the proposed model has been successfully tested using 5 MPI-DING reference glasses ranging from basalt to rhyolite,[1] plus a trachybasalt from Etna (ETN, see Di Genova *et al.*[35]) and an andesite from Montserrat (MSA).

As glassy materials are extensively dispersed on our planet, both at subaerial and submarine conditions,[36–38] and as well on extra-terrestrial bodies such as the Moon[39] and perhaps on the northern lowlands of Mars,[40] the results of our parameterization may facilitate the rapid *in situ* identification, and investigation, of silicate glasses in volcanic deposits and the remote sensing analysis of surface rocks of the terrestrial planets.

Experimental methods

The origin and nature of the samples – chaotic mixing experiments

Anhydrous and bubble-free glasses were synthesized by the melting of natural rhyolite and basalt, at 1350 °C for 4 h (see Morgavi *et al.*[41] for sample location and petrographic description). The glasses were verified to be free of crystals by optical and electron microscopy. Using a concentric cylinder setup, we determined the viscosities at 1350 °C for the basaltic and rhyolitic end-member to be 0.86 and 4.75 log Pa s, respectively.

Magma mixing was induced using the obtained samples by a chaotic mixing setup [Fig. S1 (Supporting Information)] installed at the Department of Earth and Environmental Sciences at the University of Munich (LMU, Germany). The experimental setup mimics the 'Journal Bearing Flow' configuration used by Swanson and Ottino[42] to investigate the chaotic mixing of fluids at room temperature. A detailed description of the apparatus is reported in Morgavi *et al.*[41,43] The experimental device [Fig. S1 (Supporting Information)] consists of an outer Pt_{80}-Rh_{20} cylinder and an inner Al_2O_3 cylinder covered by an outer Pt sheath. The motions of the two cylinders are independent and their rotations at given angular velocities induce chaotic magma mixing. The outer cylinder, which hosts the end-member melts, was filled with both the rhyolitic end-member (80 vol.%) and basaltic end-member (20 vol.%). The experiments were performed at 1350 °C with a duration of 108 min. This temperature has been chosen in order to produce a crystal-free and bubble-free sample and to ensure that the mixing process takes place in a rheological regime relevant for magmatic processes. After quenching, a representative section containing different mixing patterns was selected in order to perform chemical analyses [Fig. S1 (Supporting Information)].

Chemical analysis

The concentrations of major elements were measured with a Cameca SX100 electron micro probe analyzer of the Department of Earth and Environmental Sciences at the University of Munich. The chemical analyses were carried out at 15 kV acceleration voltage and 5 nA beam current. A defocused 10 μm beam was used for all elements in order to minimize alkali loss. Synthetic wollastonite (Ca, Si), periclase (Mg), hematite (Fe), corundum (Al), natural orthoclase (K), and albite (Na) were used as standards, and matrix correction was performed by PAP procedure (Pouchou and Pichoir, 1984). The precision was better than 2.5% for all analyzed elements. MnO, P_2O_5, and Cr_2O_3 contents are lower than 0.2 wt%, which is within measurements error; for this reason, these oxides are not reported in our results.

Raman spectroscopy

Raman spectra were obtained using a micro-Raman spectrometer (HORIBA; XploRa-Raman-System) equipped with three lasers (red, green, and near-infrared (NIR)). A green argon ion laser (532 nm),

Journal of RAMAN SPECTROSCOPY

which provided a power at the sample surface of ~2.5 mW, was focused through the 100× objective to an ~0.7 μm spot. The Raman system was set with a laser attenuation of 25% respect to the total laser power, 1200 T grating, exposure time 30 s (three times), confocal hole of 300 μm, and slit of 200 μm. The spatial resolution is <1 μm, while the spectral resolution is ~23 cm^{-1} (full width at half maximum). Backscattered Raman radiation was collected over a range from 50 to 1500 cm^{-1}, and elastically scattered photons were suppressed via a sharp edge filter. The instrument was calibrated using a silicon standard.

All the acquired spectra have been corrected for the wavelength of excitation source and temperature dependence of the Raman intensity according to Eqn (2) and, finally, a background subtraction technique has been applied to all the spectra.

It must be noted that the assessment of a certain baseline is a critical aspect of Raman spectra treatment, as it depends on the chemical composition of the sample and operator choices. Different authors [e.g. [30–32,44]] have reported several procedures based on empirical considerations. We have compared the different approaches, concluding that they are not appropriate for our study because our spectra are substantially different from those previously considered. In contrast to the present study, the aforementioned studies were performed using synthetic compositions.

In order to ensure the reproducibility of the background subtraction, we define two zones that are supposed free of peaks to constrain the cubic baseline: from 50 to ~250 cm^{-1} and from ~1250 to 1500 cm^{-1}. This procedure likely applies for most of the natural glasses.

Results

Optical analysis and chemical variations

Observations of the experimental products reveal that the basaltic melt was dispersed within the rhyolitic melt because of the dynamics of stretching and folding generated by the mixing experiment. Back-scattered electron (BSE) image analysis enables visualization of the chemical boundary patterns developed during mixing [Fig. S2 (Supporting Information)]. The thickness of filaments is variable in different sections of the samples, as has been previously observed from chaotic mixing dynamics.

We selected one section with a thickness of 490 μm [Fig. S2 (Supporting Information)], crossing the rhyolite–basalt contact, for further chemical analysis. Microscopic examination of the experimental products by BSE imaging reveals that the quenched-in filaments are glassy, thus preserving information about the modulation of composition during mixing due to chemical exchanges between the end-members.

The chemical composition of the analyzed transect is reported in Table S1 (Supporting Information) and is shown both as a function of distance from the rhyolitic end-member (Fig. 1) and in a total alkali silica diagram (Fig. 2). The analytical uncertainty in the chemical analysis of an individual element is reported in Table S1.

Raman spectroscopy

Figure 3 reports the Raman spectra collected from the rhyolitic to basaltic end-members together with their spatial distribution. The figure shows two main bands, one in the low-wavenumber region (LW ~250–640 cm^{-1}) and a second one in the high-wavenumber region (HW ~800–1250 cm^{-1}), which are both related to the aluminosilicate network. The LW region is usually assigned to vibrations of bridging oxygens (BO) with three-membered, four-membered, five-membered, six-membered, or higher-membered rings of tetrahedra present in silicate networks.[3,10,22–25,45–47] The HW region yields information about the vibration of T–O^- bonds [where T refers to fourfold coordinated cations (Si^{4+}, Al^{4+}, Fe^{3+}) and O^- non-bridging oxygens, NBO] and the structural effect of the

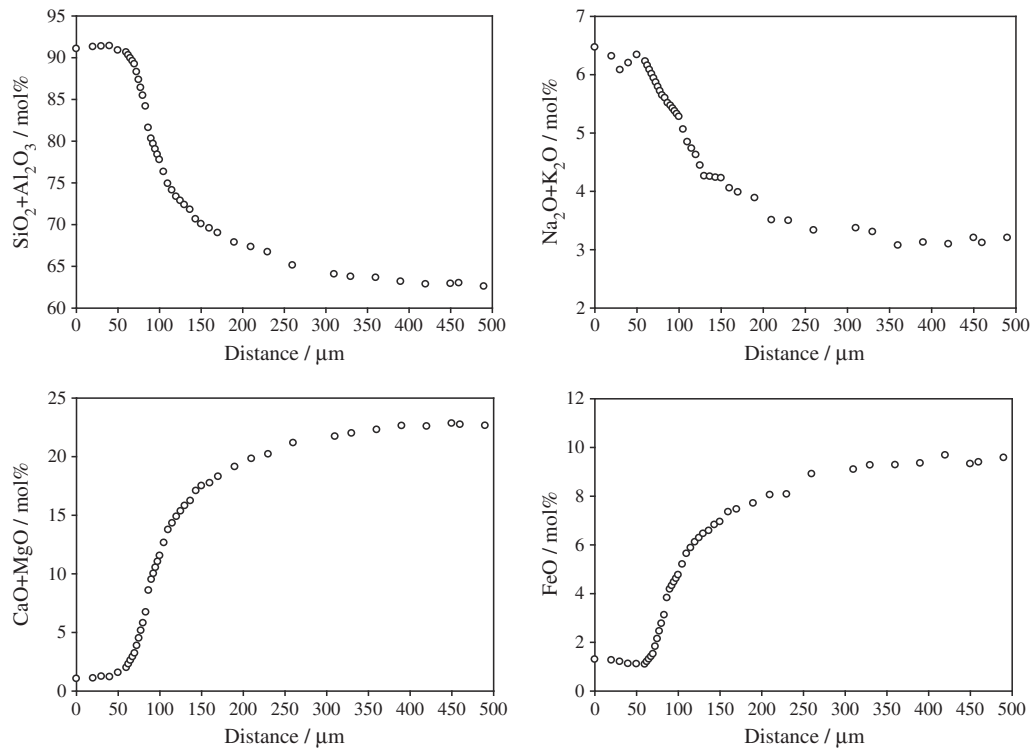

Figure 1. Measured chemical composition as a function of the distance along the analyzed filament.

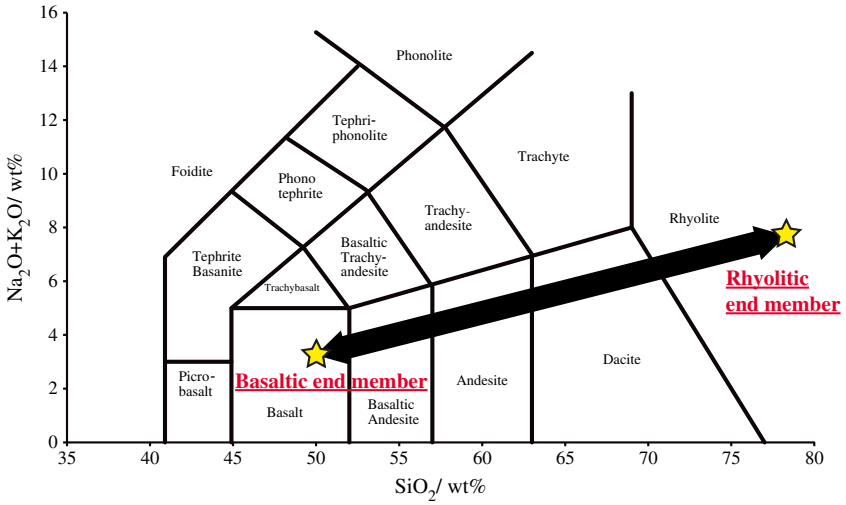

Figure 2. TAS (total alkali *vs* SiO_2 contents in wt.%) diagram showing melt compositions resulting from mixing experiments. All the samples belong to the calcalkaline magma series. The line represents the interpolation of the measured chemical composition reported in Table S1 in the Supporting Information.

network-modifying or charge balancing cations, (e.g. the works of some authors [10,25,48–53]).

The LW region from the rhyolitic end-member (Fig. 3, sample Y_12) shows one broad asymmetric band composed by three different peaks: a main peak, located at ~470 cm^{-1}, a shoulder on the left side at ~375 cm^{-1}, and a peak at ~580 cm^{-1}. With decreasing silica content, the LW Raman spectra exhibit a wider peak at ~520 cm^{-1}. The Raman spectra show a dramatic variation as the chemical composition varies toward the basaltic end-member (Y_62). In fact, differently to the Raman spectrum of Y_12 sample, the basaltic end-member shows a main broad asymmetric peak at ~525 cm^{-1} with a clear shoulder near 590 cm^{-1}, and a second weak shoulder at ~440 cm^{-1}. Overall, the intensity of the LW region is much lower than the LW intensities exhibit by the most polymerized samples.

Concerning the HW region, starting from the rhyolitic end-member (Fig. 3, sample Y_12), the spectra exhibit one broad band composed by three different peaks located at ~980, 1050, and 1150 cm^{-1}, respectively. With decreasing silica content, the collected HW Raman spectra exhibit a shift toward lower wavenumber. In fact, the basaltic end-member (Fig. 3, sample Y_62) shows a band centered at ~920 cm^{-1}, with a shoulder on its high wavenumber side at ~1000 cm^{-1}.

Discussion

Parameterization of the evolution of Raman spectra

The aims of this study include the goal of providing a database for Raman spectra of natural silicate glasses (Fig. 3) over a wide range of chemical composition (from basalt to rhyolite, along the calcalkaline series).

In order to evaluate Raman spectroscopy as a high spatial resolution tool for estimating the chemical composition of different natural glasses, we have compared the acquired Raman spectra (Fig. 3) with the measured chemical composition (Table S1).

An ideal mixing equation (Eqn (1)) was used in order to parameterize the Raman spectra as a function of the Raman parameter R_p:

$$Y = E_B \cdot R_p + E_R(1 - R_p) \quad (1)$$

where Y represents the acquired Raman spectra, and E_B and E_R represent the basalt end-member (Y_62) and rhyolite end-member (Y_12) Raman spectra, respectively. The R_p fit parameter was calculated for each acquired Raman spectra using Eqn (1) and has been reported and plotted in Table 1 and Fig. 4 as a function of chemical composition.

It must be noted that the R_p parameter is equal to 1 when only the basalt end-member is considered and, on the other hand, is equal to 0 when only rhyolite end-member is considered.

Figure 4 shows the evolution of chemical composition as a function of the R_p parameter. The different cations clearly exhibit smooth continuous trends with respect to the calculated Raman parameter.

A model to determine chemical composition of silicate glasses using Raman spectra

As stated earlier, Raman spectra and silicate structure (i.e. chemical composition) are intimately related and, for this reason, we have combined the evolution of the acquired Raman spectra with chemical composition using the calculated Raman parameter (R_p) by means of Eqn (1), obtaining an excellent correlation as illustrated in Fig. 4.

Therefore, we have parameterized the R_p parameter as a function of chemical composition (trends in Fig. 4) by adopting the following strategy:

- $SiO_2 + Al_2O_3$ content (which represent the most abundant network-forming cations) has been parameterized, using a cubic equation (Table 2, $y = b\ R_p^{\ 3} + c\ R_p^2 + d\ R_p + e$), as a function of R_p.
- CaO + MgO content has been parameterized as a function of R_p, again using a cubic equation (Table 2). As can be observed in Table S1, the mol% content of these cations continuously increases during mixing process.
- The alkaline cations show a more complex picture. Sodium shows a different trend with respect to potassium and other cations. Indeed, looking at Table S1, it can be seen that the measured Na_2O content does not change significantly during magma mixing, from the rhyolitic end-member up to sample Y_31 ($R_p = 0.781$). On the contrary, the K_2O content shows a continuous decrease from the rhyolitic to the basaltic end-member. The combination of these two different behaviors shown by Na_2O and K_2O results in the abrupt change in the

Journal of RAMAN SPECTROSCOPY

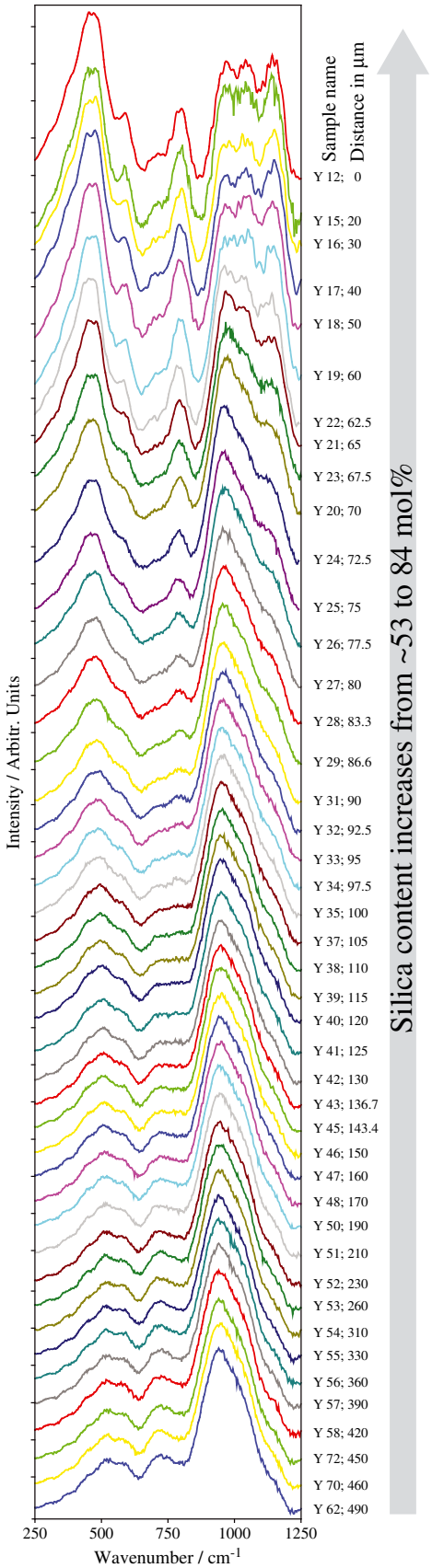

Figure 3. Long-corrected, and normalized, Raman spectra of rhyolite–basalt mixing experiment product. Labels next to each curve give the sample name and the distance in µm from the starting point (rhyolitic end-member).

Table 1. Calculated Raman parameter (R_p) using Eqn (1)

Sample	R_p	Sample	R_p
Y 12	0.000	Y 38	0.863
Y 15	0.000	Y 39	0.875
Y 16	0.000	Y 40	0.887
Y 17	0.000	Y 41	0.893
Y 18	0.162	Y 42	0.903
Y 19	0.163	Y 43	0.908
Y 22	0.217	Y 44	0.915
Y 21	0.305	Y 45	0.920
Y 23	0.422	Y 46	0.928
Y 20	0.495	Y 47	0.935
Y 24	0.559	Y 48	0.939
Y 25	0.616	Y 50	0.953
Y 26	0.653	Y 51	0.964
Y 27	0.694	Y 52	0.971
Y 28	0.715	Y 53	0.977
Y 29	0.747	Y 54	0.995
Y 30	0.762	Y 55	0.996
Y 31	0.781	Y 56	0.990
Y 32	0.796	Y 57	1.000
Y 33	0.810	Y 58	1.000
Y 34	0.819	Y 72	1.000
Y 35	0.831	Y 70	1.000
Y 37	0.851	Y 62	1.000

slope observed in Fig. 4 at R_p around 0.8, which requires the implementation of a quartic function (Table 2, $y = a R_p^4 + b R_p^3 + c R_p^2 + d R_p + e$).

- Lastly, the FeO content has been parameterized as a function of R_p parameter, using a cubic equation (Table 2).

Finally, by combining the equations reported in Table 2 with the calculated R_p parameter using Eqn (1), we can accurately estimate the chemical composition of our samples by simply using the acquired Raman spectra. In Fig. 5, we report the estimated *versus* measured chemical compositions for our samples. In addition, Fig. 6 shows a comparison between three different measured and calculated Raman spectra (Y_26, Y_40, and Y_53). From this figure, it is possible to appreciate how our model can appropriately reproduce the measured Raman spectra. The largest error in predicting a measured Raman spectrum is exhibited by the intensity of the most polymerized sample (Y_26), and we are currently investigating the silicate structure effect on Raman spectra of highly polymerized natural silicate glasses (Di Genova *et al.*, in prep.). At the same time, the wavelength position of the Raman peaks is well-predicted for all the samples. Overall, despite the small discrepancy between the measured and calculated intensity (sample Y_26), the estimation of the chemical composition is not particularly affected (Fig. 5). Finally, as will be discussed later, we are planning to further develop our model including different end-members to improve the reproducibility of the measured Raman spectra.

Effect of iron oxidation state on Raman spectra of natural silicate glasses

As previously discussed, our mixing experiment was performed in oxidizing conditions. However, the magmas, and as a consequence the natural glasses, do not necessarily have a high oxidation state.

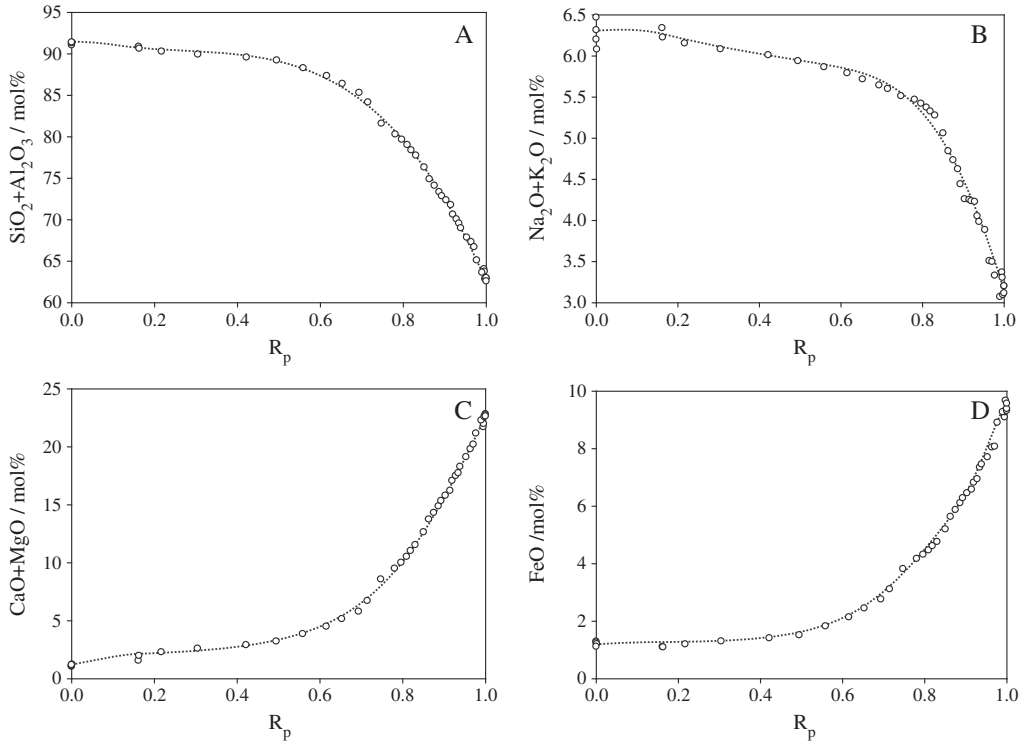

Figure 4. Measured chemical composition as a function of the calculated Raman parameter (R_p) using Eqn (1). Lines represent the fits obtained using equations reported in Table 2.

Table 2. Equation and fit parameters used to parameterize the chemical composition (y, in mol%) as a function of the Rp parameter: $y = aR_p^4 + bR_p^3 + cR_p^2 + dR_p + e$

	a	b	c	d	e	R^2
$SiO_2 + Al2O_3$	0	−63.749	47.071	11.651	91.327	0.999
CaO + MgO	0	50.754	−40.686	11.560	1.095	0.999
FeO	0	19.383	−13.906	2.710	1.163	0.997
$Na_2O + K_2O$	−18.419	26.492	−12.538	1.281	6.272	0.991

In addition, it is well-known that the iron redox state can affect the silicate structure, and therefore both the related physical properties (i.e. viscosity, density, and heat capacity) and Raman spectrum in a complex way. Most data concerning the influence of iron and its redox state on these properties deal with simple synthetic systems.[54–57] Even though the literature related to the effect of iron oxidation state on the structure of natural silicate glasses is still poor, one study[58] has investigated the effect of variable $Fe^{3+}/\Sigma Fe_{tot}$ ratios on Raman spectra of natural iron-bearing glasses. The investigated samples are represented by a pantellerite (peralkaline iron-rich rhyolite) characterized by a total iron content of 7.8 wt.% and two basalts, one iron-poor and one iron-rich (FeO_{tot} 7.6 and 10.1 wt.%, respectively). The authors reported how the sensitivity of glass structure to iron redox decreases with increasing glass basicity. In fact, the Raman spectra of basaltic samples does not exhibit any appreciable variation as a function of different $Fe^{3+}/\Sigma Fe_{tot}$ ratios. On the contrary, the Raman spectra of rhyolitic glasses show an increase of a band at ~970 cm^{-1} with the $Fe^{3+}/\Sigma Fe_{tot}$ ratio.

As can be observed from Table S1, our rhyolitic end member has a low iron content (1.2 wt.%), extremely lower than the iron content showed by the sample used in Di Muro *et al.*[58] For this reason, we

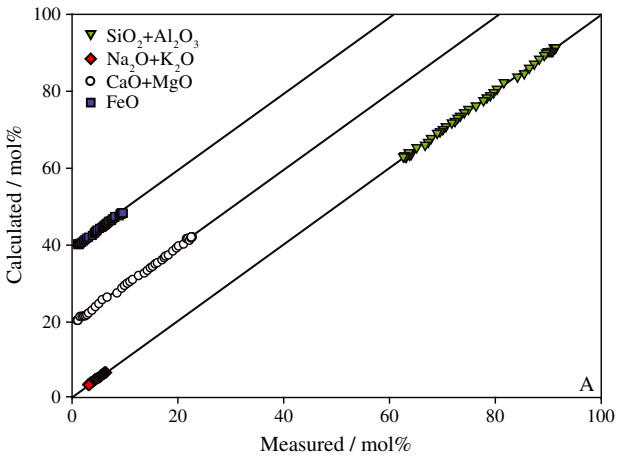

Figure 5. Comparison between measured and calculated chemical composition using the proposed Raman model. To better visualize the reported date, the calculated CaO + MgO and FeO have been shifted of 20 and 40 mol%, respectively.

believe that the Raman spectra of our rhyolitic samples are not substantially affected by the Fe^{2+}/Fe_{tot} ratio, extending the applicability of our model to magmatic conditions. However, it is important to point out that our model cannot be used to estimate the chemical composition of samples belonging to the peralkaline iron-rich system, as the Raman spectrum is affected by the Fe^{2+}/Fe_{tot} ratio.

Validation of the model

In order to validate our approach, we have investigated further samples and, in addition, tested the possible influence of Raman

Journal of RAMAN SPECTROSCOPY

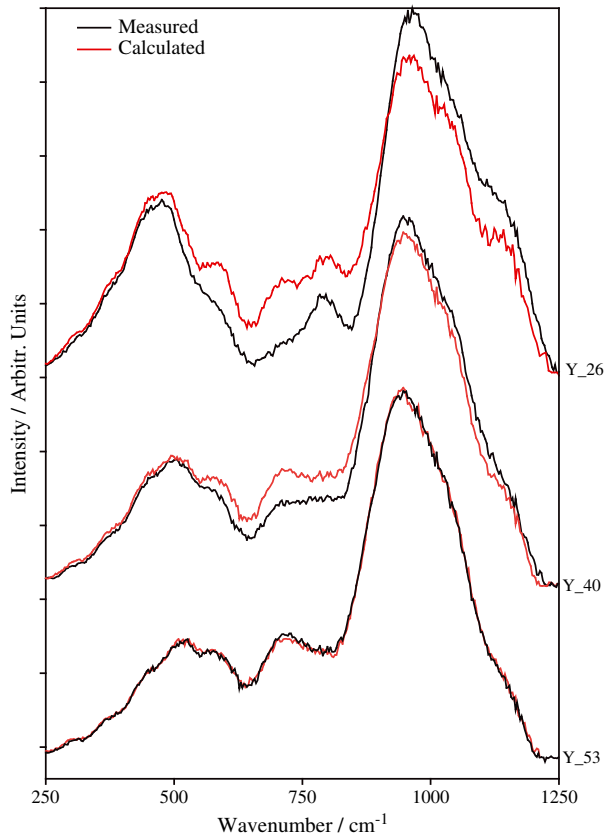

Figure 6. Comparison between measured and calculated Raman spectra (Y_26, 40, 53) using the proposed Raman model (Eqn (1)).

spectra acquisition conditions on our results. For this purpose, we have used seven natural standard glasses: five MPI-DING glasses from Jochum *et al.*[1]; a remelted trachybasalt from ETN (Di Genova *et al.*[35]); and a remelted andesite from MSA. In Table 3, the chemical compositions are reported, and it must be noticed that all of the samples belong to the calcalkaline magma series, with the only exception of ETN sample, which is rich in sodium.

Main experimental conditions for Raman analysis include the following: laser device 532 nm, laser energy attenuation of 25%–50%, grating 1200 T, confocal hole 100–300 μm, slit 200, observation objective × 100, and exposure time 30–40 s.

The acquired Raman spectra are reported in Fig. 7. In Table 3, we report, for each sample, the calculated R_p parameters using Eqn (1), the measured chemical composition, and the calculated chemical composition using our model (equations in Table 2) together with the calculated polymerization degree expressed as non-bridging oxygen per tetrahedra (NBO/T on a molar basis according to Mysen.[59] In order to calculate the NBO/T parameter, the measured total iron (FeO_{tot}) was split 75% as Fe_2O_3 and 25% as FeO. This is a sensible assumption as the mixing experiment was performed in oxidizing condition in air. Under this condition, ferric iron is predominantly in tetrahedral coordination in silicate glasses (e.g. Mysen *et al.*[60]).

It is interesting to point out that our Raman parameter (R_p) can be used as a proxy to discern the polymerization degree of the investigated silicate glasses. In fact, looking at Table 3, for a low value of NBO/T corresponds a low value of R_p. In particular, the ATHO-G sample (rhyolite) exhibits both the lowest value of NBO/T (0.01) and R_p (0.488) among the analyzed samples. At the same time the KL2-G sample (basalt) is characterized by both the highest value of NBO/T (0.58) and R_p (1) with respect to the other samples.

Table 3. Literature and calculated chemical composition (normalized in mol%) of analyzed external samples used to test the proposed Raman model

			Measured	Calculated		Measured	Calculated		Measured	Calculated	
Sample	R_p[a]	NBO/T[b]	$SiO_2 + Al_2O_3$	$SiO_2 + Al_2O_3$	Δ[c]	$Na_2O + K_2O$	$Na_2O + K_2O$	Δ[c]	CaO + MgO	CaO + MgO	Δ[c]	FeO	FeO	Δ[c]
ATHO-G[d]	0.488 (± 0.016)	0.01	89.21 (± 0.6)	89.45 (± 0.2)	−0.23	5.52 (± 0.2)	5.94 (± 0.4)	−0.42	2.08 (± 0.1)	2.94 (± 0.1)	−0.87	3.01 (± 0.1)	1.43 (± 0.1)	1.59
StHs6/80-G[d]	0.689 (± 0.011)	0.10	80.42 (± 0.3)	84.81 (± 0.4)	−4.39	5.64 (± 0.1)	5.72 (± 0.5)	−0.20	9.32 (± 0.1)	6.34 (± 0.3)	2.99	3.95 (± 0.1)	2.76 (± 0.1)	1.19
MSA[e]	0.797 (± 0.007)	0.16	75.67 (± 0.3)	79.65 (± 0.5)	−3.98	4.50 (± 0.1)	5.31 (± 0.6)	−0.81	13.54 (± 0.2)	10.17 (± 0.4)	−0.99	5.62 (± 0.1)	5.75 (± 0.2)	−0.13
T1-G[d]	0.819 (± 0.009)	0.20	74.48 (± 0.3)	78.35 (± 0.6)	−3.87	4.66 (± 0.1)	5.18 (± 0.6)	−0.52	13.94 (± 0.1)	11.14 (± 0.4)	2.80	5.84 (± 0.1)	4.70 (± 0.2)	1.14
ML3B-G[d]	0.989 (± 0.002)	0.51	63.10 (± 0.2)	64.21 (± 0.2)	−1.11	2.71 (± 0.1)	3.27 (± 0.6)	−0.56	22.57 (± 0.2)	21.81 (± 0.2)	0.76	9.79 (± 0.1)	8.98 (± 0.5)	0.81
ETN[f]	0.997 (± 0.003)	0.44	63.24 (± 0.3)	63.32 (± 0.2)	−0.08	5.18 (± 0.1)	3.12 (± 0.6)	2.06	20.62 (± 0.2)	22.48 (± 0.3)	−1.86	9.06 (± 0.2)	9.25 (± 0.1)	−0.19
KL2-G[d]	1.000 (± 0.003)	0.58	61.66 (± 0.2)	63.00 (± 0.3)	−1.34	2.67 (± 0.1)	3.07 (± 0.4)	−0.40	24.13 (± 0.2)	22.72 (± 0.4)	1.17	9.55 (± 0.1)	9.35 (± 0.1)	0.20

[a]Calculated Raman parameter using Eqn (1).
[b]Mysen[60]
[c]Difference between measured and calculated chemical composition.
[d]Jochum *et al.*[1]
[e]This study.
[f]Di Genova *et al.*[35]
Literature and calculated chemical composition (normalized in mol%) of analyzed

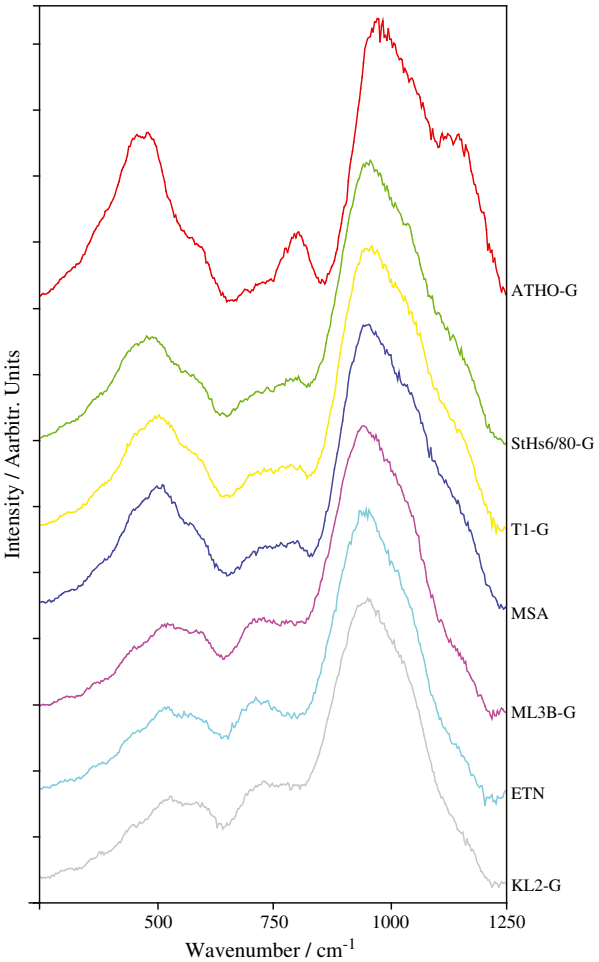

Figure 7. Long-corrected, and normalized, Raman spectra of samples used to validate our Raman model. MPI-DING glasses from Jochum[1]; Etna (ETN) from Di Genova *et al.*[35]; and Montserrat (MSA) from this study.

Figure 8 shows the complete relation between the calculated NBO/T and R_p parameter.

Further, our parameter shows a higher sensitivity than NBO/T in distinguishing different highly polymerized (i.e. evolved) silicate glasses. In fact, both the ATHO-G and Y_12 rhyolites are characterized by the same NBO/T = 0 but different R_p parameter (0.488 and 0, respectively). As can be seen, looking at Tables S1 and 3, the Y_12 is chemically more evolved compared with the ATHO-G rhyolite, and this is well in accordance with the calculated $R_p = 0$ for the Y_12 sample. In particular, the Y_12 rhyolite shows a higher $SiO_2 + Al_2O_3$ content (91.06 mol%), while the sum of alkali and alkaline earth content is clearly lower (5.58 mol%) than the ATHO-G rhyolite, which in turn exhibits 89.45 and 7.60 mol%, respectively.

As the proposed Raman parameter is highly sensitive to the chemical composition of a silicate glass, we believe that this parameter may represent a valuable tool to investigate the differentiation process of natural silicate melts. In addition, as shown in Table 3, the basaltic sample KL2-G is more mafic than our basaltic end-member (Y_62). Indeed, the $SiO_2 + Al_2O_3$ content for KL2-G sample is 61.66 mol%, lower than the measured value for the sample Y_62 (63.00 mol%). For this reason, our model cannot predict a $SiO_2 + Al_2O_3$ content lower than 63.00 mol% and, as a consequence of that, both samples are characterized by a value of R_p equal to 1. On account of this, a possible further development of our model has to take into account the KL2-G as a basaltic end-member

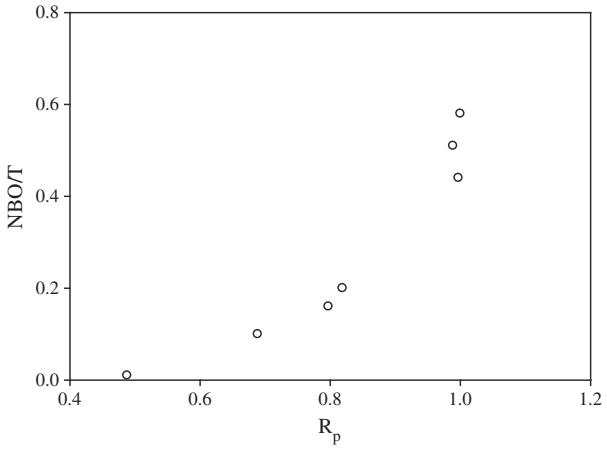

Figure 8. Non-bridging oxygen per tetrahedra (NBO/T) on a molar basis according to Mysen[57] *versus* the calculated Raman parameter (R_p, Eqn (1)). The degree of polymerization of the analyzed samples increases with the calculated Raman parameter.

instead of the sample Y_62, in order to expand the measurable $SiO_2 + Al_2O_3$ content via Raman spectroscopy.

Looking carefully at Table 3, it is possible to assess quantitatively the validity of our model to determine the chemical composition of silicate glasses. Additionally, a comparison between the calculated and the measured chemical composition of the additional samples investigated is reported in Fig. 9. As can be seen in the figure, within the standard error of estimation, the calculated chemical compositions of the investigated sample are well in accordance with the measured chemical compositions.

In particular, as for the intermediate compositions (two andesites and a qz-diorite), our model slightly overestimate the measured $SiO_2 + Al_2O_3$ content (~5%). Concerning the $Na_2O + K_2O$ content, the ETN basalt shows the largest error. A possible explanation for this resides in the high alkali content of Etna's basalts, much higher (5.18 mol% respectively) compared with that shown by our basaltic end-member Y_62 (3.20 mol%).

Regarding the CaO + MgO and FeO content, the model exhibits the largest errors in determining the chemical composition when the ATHO-G rhyolite and STHS6/80-G andesite are

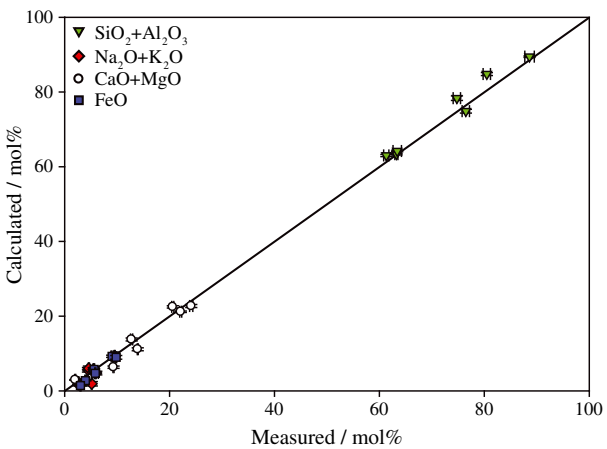

Figure 9. Comparison between measured and calculated chemical composition using the proposed Raman model for the external samples used to test the proposed Raman model.

considered. Again, a possible explanation for this might be related to the chemical composition of our rhyolitic end-member, which largely affects the estimation of iron and alkaline earth content for the most evolved samples. In fact, for example, the Y_12 sample is extremely poor in iron (1.3 mol%) and alkaline earth content (1.05 mol%) compared with the chemical composition of ATHO-G rhyolite and STHS6/80-G andesite (3.01–2.08 and 3.95–9.32 mol%, respectively).

For this reason, we are planning to further develop our model including several end-members able to take into account the chemical heterogeneities of silicate glasses, resulting from the different volcanological settings.

How to use the model

The Excel© version of our model is provided as Supporting Information. First of all, a Raman spectrum has to be acquired, and we suggest setting the Raman system on how it is reported in paragraph 2.3.

Subsequently, the following correction has to be applied to the acquired Raman spectrum (see Long[61] for the theoretical background):

$$I = I_{obs} \cdot \left\{ \nu_0^3 \cdot \nu \frac{[1 - \exp(-hc\nu/kT)]}{(\nu_0 - \nu)^4} \right\} \quad (2)$$

where I_{obs} is the acquired Raman spectra, *h* is the Planck constant, $h = 6.62607 \times 10^{-34}$ J s, k is the Boltzmann constant; $k = 1.38065 \times 10^{-23}$ J K^{-1}, c is the speed of light, $c = 2.9979 \times 10^{10}$ cm s^{-1}, T is the absolute temperature, ν_0 is the wavenumber of the incident laser light (10^7/532 for the green laser), and ν is the measured wavenumber in cm^{-1}.

After applying the Long's correction, the background subtraction has to be applied to the acquired spectrum (see paragraph 2.3). Then, an intensity normalization to 100 (arbitrary units) must be applied to the spectrum.

Finally, before using the Excel© file, it is important to verify that the three different Raman spectra (two end-members spectra Y_12 and Y_62 and the sample spectrum) have to be necessarily characterized by the same X values (cm^{-1}).

Conclusions and perspectives

Here, the first database of natural silicate glasses is presented together with a Raman model to estimate the degree of polymerization and the chemical composition of natural silicate glasses for calcalkaline compositions (Table S1).

The database and the model together represent a high spatial resolution (~1 μm) tool for a quick *in situ*, and remotely controlled, identification of silicate glasses dispersed in rocks and volcanic deposits. Additionally, the proposed Raman model is based on an ideal mixing equation that avoids the use of deconvolution bands, for which assignment is still strongly debated in literature.[10,34]

The model has been first applied to remelted natural samples and is independent on Raman acquisition conditions. In future works, it will be tested and improved, performing new experimental measurements on samples with different geochemical compositions in order to cover the chemical variability of natural magmatic compositions. These new measurements will be performed in order to take into account both the effect of the excess alkalies over aluminum, iron content, and oxygen fugacity on the Raman spectra of silicate glasses.

This study represents a new tool for *in situ* volcanology and planetary science (e.g. ExoMars program). Indeed, in the last years, Raman spectroscopy has been recognized as a promising tool for *in situ* and/or remote investigation of organic and inorganic material of bodies in our solar system.[5,62–65] In particular, it has been demonstrated that Raman spectroscopy can be used both *in situ* and in remote conditions up to 100 m [e.g. [66,67]] as a method to infer qualitatively the composition of samples. Our study extends the potential use of Raman spectroscopy to quantify the chemical composition, and polymerization degree, of silicate glasses. In fact, silicate glasses have been found, and are supposed to be largely dispersed, on planetary bodies.[39,40,68–70] The use of parameterization might help in shedding new light on the type of magmatism and volcanic activity in our solar system (as well as on the formation of impact craters).

Acknowledgements

This research was funded by the European Union's Seventh Programme for research technological development and demonstration under grant agreement No 282759 – VUELCO and by the ERC Consolidator Grant 612776 – CHRONOS and by the ERC Advanced Grant 247076 – EVOKES. The authors are grateful to Dr S. Ferrero, Dr Francesca Tecce, and Prof. M. L. Frezzotti for useful discussions and advice. We thank Dr Philippe Colomban and three anonymous reviewers for constructive comments to the manuscript. The first author wishes to thank S. Fleckenstein, M. Cinque, F. Reith, and I. K. Curtis for the illuminating discussion and encouraging support.

References

[1] K. P. Jochum, D. B. Dingwell, A. W. Hofmann, A. Rocholl, B. Stoll, *Geostand. Geoanal. Res.* **2000**, *24*, 87.
[2] H. L.Welsh, M. F. Crawford, T. R. Thomas, G. R. Love, *Can. J. Phys.* **1952**, *30*, 577.
[3] P. F. McMillan, B. Piriou, *J. Non-Cryst. Solids* **1982**, *53*, 279.
[4] B. O. Mysen, J. D. Frantz, *Geochim. Cosmochim. Acta* **1994**, *58*, 1711.
[5] N. Tarcea, T. Frosch, P. Rösch, M. Hilchenbach, T. Stuffler, S. Hofer, H. Thiele, R. Hochleitner, J. Popp, *Space Sci. Rev.* **2008**, *135*, 281.
[6] L. M. Malard, M. A. Pimenta, G. Dresselhaus, M. S. Dresselhaus, *Phys. Rep.* **2009**, *473*, 51.
[7] M. M. Mariani, P. J. R. Day, V. Deckert, *Integr. Biol.* **2010**, *2*, 94.
[8] J. Dubessy, M. C. Caumon, F. Rull, S. Sharma, *Raman Spectrosc. Appl. to Earth Sci. Cult. Herit.* **2012**, *83*.
[9] A. F. Goncharov, *Int. J. Spectrosc.* **2012**, 1–16.
[10] D. R. Neuville, D. de Ligny, G. S. Henderson, *Rev. Mineral.* **2014**, *78*, 509.
[11] P. Colomban, *J. Non-Cryst. Solids* **2003**, *323*, 180.
[12] P. Colomban, O. Paulsen, *J. Am. Ceram. Soc.* **2005**, *88*, 390.
[13] L. Robinet, A. Bouquillon, J. Hartwig, *J. Raman Spectrosc.* **2008**, *39*, 618.
[14] P. Colomban, *J. Raman Spectrosc.* **2012**, *43*, 1529.
[15] I. B. Hutchinson, R. Ingley, G. M. Howell, L. Harris, M. Mchugh, C. Malherbe, J. Parnell, *Philos. Trans. R. Soc. London* **2014**, 372.
[16] P. Vandenabeele, H. G. M. Edwards, J. Jehlička, *Chem. Soc. Rev.* **2014**, *43*, 2628.
[17] J. D. Pasteris, B. Wopenka, P. G. Brewer, S. N. White, E. T. Peltzer, G. E. Malby, *Appl. Spectrosc.* **2004**, *58*, 195.
[18] J. F. Scott, S. P. S. Porto, *Phys. Rev.* **1967**, *161*, 903.
[19] C. Y. She, J. D. Masso, D. F. Edwards, *J. Phys. Chem. Solids* **1971**, *32*, 1887.
[20] E. Balan, D. R. Neuville, P. Trocellier, E. Fritsch, J. P. Muller, G. Calas, *Am. Mineral.* **2001**, *86*, 1025.
[21] R. J. Bell, N. F. Bird, P. Dean, *J. Phys. C.* **1968**, *1*, 299.
[22] F. Seifert, B. O. Mysen, D. Virgo, *Am. Mineral.* **1982**, *67*, 696.
[23] P. F. McMillan, G. H. Wolf, Vibrational spectroscopy of silicate liquids, in Structure, Dynamics and Properties of Silicate, Mineralogical Society of America, **1995**, *33*, 247–315.
[24] D. R. Neuville, B. O. Mysen, *Geochim. Cosmochim. Acta* **1996**, *96*, 1727.

[25] B. O. Mysen, *Eur. J. Mineral.* **2003**, *15*, 781.
[26] M. Mercier, A. Di Muro, N. Métrich, D. Giordano, O. Belhadj, C. W. Mandeville, *Geochim. Cosmochim. Acta* **2010**, *19*, 5641.
[27] M. L. Frezzotti, F. Tecce, A. Casagli, *J. Geochem. Explor.* **2012**, *112*, 1.
[28] R. Thomas, P. Davidson, *Zeitschrift der Dtsch. Gesellschaft für Geowissenschaften* **2012**, *163*, 113.
[29] Z. Zajacz, W. Halter, W. J. Malfait, O. Bachmann, R. J. Bodnar, M. M. Hirschmann, C. W. Mandeville, Y. Morizet, O. Müntener, P. Ulmer, J. D. Webster, *Contrib. Mineral. Petrol.* **2005**, *150*, 631.
[30] H. Behrens, J. Roux, D. R. Neuville, M. Siemann, *Chem. Geol.* **2006**, *229*, 96.
[31] M. Mercier, A. Di Muro, D. Giordano, N. Métrich, P. Lesne, M. Pichavant, B. Scaillet, R. Clocchiatti, G. Montagnac, *Geochim. Cosmochim. Acta* **2009**, *73*, 197.
[32] C. Le Losq, D. R. Neuville, R. Moretti, J. Roux, *Am. Mineral.* **2012**, *97*, 779.
[33] Y. Morizet, R. A. Brooker, G. Iacono-Marziano, B. A. Kjarsgaard, *Am. Mineral.* **2013**, *98*, 1788.
[34] S. Rossano, B. O. Mysen, Raman spectroscopy of silicate glasses and melts in geological systems. EMU Notes in Mineralogy, 12, **2012**.
[35] D. Di Genova, C. Romano, D. Giordano, M. Alletti, *Geochim. Cosmochim. Acta* **2014**, *142*, 314.
[36] W. B. Bryan, J. G. Moore, *Geol. Soc. Am. Bull.* **1977**, *88*, 556.
[37] F. A. Frey, N. Walker, D. Stakes, S. R. Hart, R. Neilsen, *Earth Planet. Sci. Lett.* **1993**, *115*, 117.
[38] K. Heide, G. Heide, *Chem. der Erde* **2011**, *71*, 305.
[39] C. K. Shearer, J. J. Papike, S. B. Simon, N. Shimizu, H. Yurimoto, S. Sueno, *Geochim. Cosmochim. Acta* **1990**, *54*, 851.
[40] B. Horgan, J. F. Bell, *Geol.* **2012**, *40*, 391.
[41] D. Morgavi, D. Perugini, C. P. De Campos, W. Ertel-Ingrisch, D. B. Dingwell, *J. Volcanol. Geotherm. Res.* **2013**, *253*, 87.
[42] P. D. Swanson, J. M. Ottino, *J. Fluid Mech.* **1990**, *213*, 227.
[43] D. Morgavi, D. Perugini, C. P. De Campos, W. Ertl-Ingrisch, Y. Lavallée, L. Morgan, D. B. Dingwell, *Chem. Geol.* **2013**, *346*, 199.
[44] Y. Zhang, H. Ni, *Rev. Mineral. Geochem.* **2010**, *72*, 171.
[45] B. O. Mysen, D. Virgo, C. M. Scarfe, *Am. Mineral.* **1980**, *65*, 690.
[46] A. Pasquarello, J. Sarnthein, R. Car, *Phy. Rev. B* **1998**, *57*, 14133.
[47] P. Umari, X. Gonze, A. Pasquarello, *Phys. Rev. Lett.* **2003**, *90*, 027401.
[48] J. Bell, P. Dean, *Philos. Mag.* **1972**, *25*, 1381.
[49] T. Furukawa, K. E. Fox, W. B. White, *J. Chem. Phys.* **1981**, *75*, 3226.
[50] P. F. McMillan, *Am. Mineral.* **1984**, *69*, 645.
[51] B. O. Mysen, M. J. Toplis, *Am. Mineral.* **2007**, *92*, 933.
[52] C. Le Losq, D. R. Neuville, *Chem. Geol.* **2013**, *346*, 57.
[53] C. Le Losq, D. R. Neuville, P. Florian, G. S. Henderson, D. Massiot, *Geochim. Cosmochim. Acta* **2014**, *126*, 495.
[54] B. O. Mysen, D. Virgo, F. Seifert, *Am. Mineral.* **1984**, *69*, 834.
[55] D. B. Dingwell, D. Virgo, *Geochim. Cosmochim. Acta* **1988**, *52*, 395.
[56] V. Magnien, D. R. Neuville, L. Cormier, J. Roux, J.-L. Hazemann, D. de Ligny, S. Pascarelli, I. Vickridge, O. Pinet, P. Richet, *Geochim. Cosmochim. Acta* **2008**, *72*, 2157.
[57] M. O. Chevrel, D. Giordano, M. Potuzak, P. Courtial, D. B. Dingwell, *Chem. Geol.* **2013**, *346*, 93.
[58] A. Di Muro, N. Métrich, M. Mercier, D. Giordano, D. Massare, G. Montagnac, *Chem. Geol.* **2009**, *259*, 78.
[59] B. O. Mysen, *Structure and Properties of Silicate Melts*, Elsevier Publishing Company, Amsterdam, **1988**.
[60] B. O. Mysen, D. Virgo, C. M. Scarfe, D. J. Cronin, *Am. J. Sci.* **1985**, *70*, 487.
[61] D. A. Long, *Mcgraw-Hill* **1977**, *2*, 276.
[62] A. Ellery, D. Wynn-Williams, *Astrobiology* **2003**, *3*.
[63] A. Wang, *J. Geophys. Res.* **2003**, *108*, 5005.
[64] V. Klein, J. Popp, N. Tarcea, M. Schmitt, W. Kiefer, S. Hofer, T. Stuffler, M. Hilchenbach, D. Doyle, M. Dieckmann, *J. Raman Spectrosc.* **2004**, *35*, 433.
[65] N. Bost, C. Ramboz, N. LeBreton, F. Foucher, G. Lopez-Reyes, S. De Angelis, M. Josset, G. Venegas, A. Sanz-Arranz, F. Rull, J. Medina, J.-L. Josset, A. Souchon, E. Ammannito, M. C. De Sanctis, T. Di Iorio, C. Carli, J. L. Vago, F. Westall, *Planet. Space Sci.* **2015**, *1*.
[66] S. K. Sharma, S. Ismail, S. M. Angel, P. G. Lucey, C. P. McKay, A. K. Misra, P. J. Mouginis-Mark, H. Newsom, E. R. D. Scott, U. N. Singh, G. J. Taylor, *Instruments, Science, and Methods for Geospace and Planetary Remote Sensing* **2004**, *128*, 128.
[67] J. D. Stopar, P. G. Lucey, S. K. Sharma, A. K. Misra, G. J. Taylor, H. W. Hubble, *Spectrochim. Acta A Mol. Biomol. Spectrosc.* **2005**, *61*, 2315.
[68] D. Stöffler, *J. Non Cryst. Solids* **1984**, *67*, 465.
[69] R. Kallenbach, J. Geiss, W. K. Hartmann, *Chronology and evolution of Mars* **2001**, 499.
[70] P. H. Schultz, J. F. Mustard, *J. Geophys. Res.* **2004**, 109.

Supporting Information

Additional supporting information may be found in the online version of this article at the publisher's web site.

Figure S1: (A) Schematic 3D-model and (B) 2D section of the experimental apparatus used to perform chaotic mixing experiments. In the figure, experimental parameters are also reported (C). Their values are as follows: $R_{out} = 13$ mm, $\Omega_{out} = 0.06$ rpm, $R_{in} = 4.3$ mm, $\Omega_{in} = 0.3$ rpm, $d = 3.9$, $r = 5.0$ mm.

Figure S2: Back-scattered electron image (BSE) of the analyzed filament. The mixing experiments were performed at 1350 °C with a duration of 108 min, using rhyolite (dark gray) and basalt (light gray).